Rapid Communications

Anomalous thermal expansion and chiral phonons in BiB_3O_6

Carl P. Romao *

Department of Chemistry, University of Oxford, Inorganic Chemistry Laboratory, South Parks Road, Oxford OX1 3QR, United Kingdom and Section for Solid State and Theoretical Inorganic Chemistry, Institute of Inorganic Chemistry, University of Tübingen, Auf der Morgenstelle 18, D-72076 Tübingen, Germany

(Received 28 February 2019; revised manuscript received 1 August 2019; published 21 August 2019)

The origins of anomalous thermal expansion in the chiral monoclinic solid α-BiB_3O_6 have been studied through *ab initio* calculations. Positive and negative axial thermal expansion are shown to be driven by librations of borate units, elastic anisotropy, and most notably by chiral acoustic phonons involving elliptical motions of bismuth atoms. The chirality of the lattice gives rise to these modes by allowing the transverse acoustic branches to have opposite circular polarizations, only one of which couples strongly to the lattice strains. These results further the understanding of relationships between crystallographic symmetry and physical properties.

DOI: 10.1103/PhysRevB.100.060302

The monoclinic α phase of bismuth borate (BiB_3O_6), in addition to having promising applications in nonlinear optics [1,2] and quantum computing [3,4], possesses the unusual physical properties of uniaxial negative thermal expansion (NTE) [5,6] and negative linear compressibility (NLC) [7,8] (Fig. 1). The chiral $C2$ space group adopted by α-BiB_3O_6 [6] has unusually low symmetry for an NTE material [9,10], or indeed more generally for an inorganic solid. The chirality of α-BiB_3O_6 permits it to have chiral phonons, i.e., phonons with a circular polarization and pseudoangular momentum [11–13]. Phonon pseudoangular momentum can interact with the electron magnetic moment [14–17], and can couple thermal gradients to the angular momentum of bulk crystals [18]. In diamagnetic systems, phonon anharmonicity is known to be affected by chirality in two ways: through the valley phonon Hall effect [11], and through modification of the symmetry constraints for scattering [19]. However, these previous studies were limited to one-dimensional (1D) and 2D materials. The anharmonic effects of phonon chirality are studied here in a diamagnetic 3D crystal through their relationship with thermal expansion [20].

The thermal expansion of α-BiB_3O_6 is highly anisotropic, with large NTE along **a** and large positive thermal expansion along **b** [5,6]. Such behavior is characteristic of flexible framework materials, i.e., materials which have a mixture of compliant and stiff directions. Indeed, α-BiB_3O_6 is also very elastically anisotropic: in the **ac** plane the ratio of Young's moduli between the stiffest and most compliant direction (Y_{max}/Y_{min}) is 25 [Fig. 1(b)]; in the **ab** plane $Y_{max}/Y_{min} = 15$ [Fig. 1(d)] [5]. By these standards, α-BiB_3O_6 is an extraordinarily flexible inorganic material; it can be compared to the colossal NTE material $Ag_3[Co(CN)_6]$, for which $Y_{max}/Y_{min} = 6.0$ [21,22], and to $ZnAu_2(CN)_4$, which exhibits extreme NLC and has $Y_{max}/Y_{min} = 3.8$ [23].

Axial NTE has been studied extensively in the tetragonal, orthorhombic, and hexagonal crystal families due to the appearance of anomalously large-magnitude thermal expansion [22], connections with ferroelectricity [24,25], and the use of chemical control to achieve zero thermal expansion [26]. However, NTE is extremely rare in monoclinic and triclinic crystals [9,10]. Outside of α-BiB_3O_6, the phenomenon has only been studied in molecular crystals, where the mechanism commonly involves the sliding of layers relative to each other [27,28]. Elastic interactions between layers in α-BiB_3O_6 are strong in the direction coinciding with Bi–O bonds, and thermal expansion has a small positive value in that direction

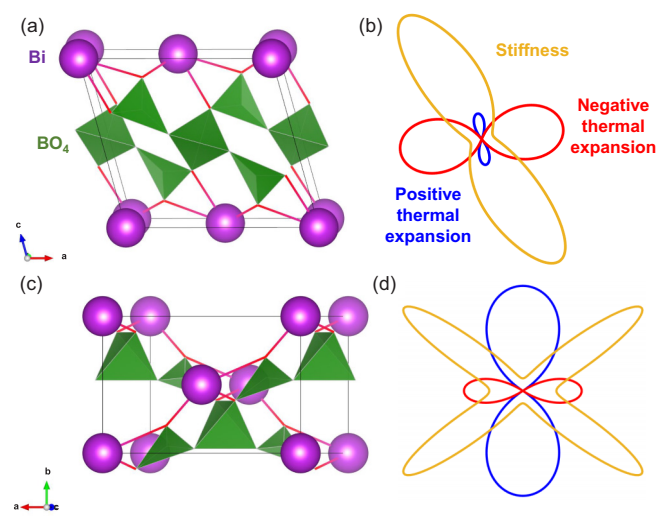

FIG. 1. At left, the structure of α-BiB_3O_6 is shown in the **ac** plane (a) and the **ab** plane (c), with bismuth atoms colored in magenta and borate units colored in green [6]. At right [(b),(d)], the indicatrix of directional Young's modulus is shown in orange, and those of positive and negative thermal expansion are shown in blue and red, respectively [5,7]. Strong elastic couplings (i.e., directions with large Young's moduli) are found both between (b) and within (d) layers, indicating that α-BiB_3O_6 is a flexible 3D framework material, with large-magnitude directional thermal expansion along the most compliant directions.

*carl.romao@mnf.uni-tuebingen.de

[Fig. 1(b)]; α-BiB_3O_6 therefore offers a unique opportunity to study NTE in a chiral monoclinic 3D framework solid.

Herein is reported a theoretical investigation of the origins of anomalous thermal expansion in α-BiB_3O_6, and of the influence of phonon chirality on this bulk property. The contribution of individual phonons to thermal expansion was assessed following the method of Ref. [29]; i.e., using uniaxial stress perturbations to calculate mode Grüneisen parameters ($\gamma_{ij,n,\mathbf{k}}$):

$$\gamma_{ij,n,\mathbf{k}} = -\frac{1}{s_{ijij}}\left(\frac{\partial \ln \omega_{n,\mathbf{k}}}{\partial \sigma_{ij}}\right)_{T,\sigma'}, \tag{1}$$

where $\mathbf{s}$ is the elastic compliance tensor. These mode Grüneisen parameters were averaged, weighted by their contribution to the heat capacity (C_e), to give bulk Grüneisen parameters (γ_{ij}), and subsequently determined directional coefficients of thermal expansion (CTEs, α_{ij}) as [29]

$$\alpha_{ij} = s_{ijij}\gamma_{ij}\frac{C_e}{V}. \tag{2}$$

This recently developed method relates each mode Grüneisen parameter to the thermal expansion in a single direction, and therefore allows identification of the phonons which drive thermal expansion along each principal axis [29].

Phonon band structures and the elastic tensor were calculated using density functional theory (DFT) [30,31] within the software package ABINIT [32–35]; example input files are available as part of the Supplemental Material [36]. The uniaxial stress perturbations used were σ_{11}, σ_{22}, σ_{33}, and σ_{13}; the Cartesian axes **x** and **y** coincide with the lattice vectors **a** and **b**, respectively, and the **z** axis is therefore the stacking direction of the borate layers [Fig. 1(a)]. DFT methods were validated by comparison of calculated elastic and thermal expansion tensors to experimental values [5,7]. As described in the Supplemental Material [36], several approaches were trialed [37–45]. The most accurate results were found for a dispersion-corrected exchange–correlation functional [39,40]; the calculations underestimated the magnitude of thermal expansion somewhat but were able to qualitatively reproduce the experimental behavior [36].

The calculated directional Young's moduli ($Y_{ii} = 1/s_{iiii}$) are shown in Fig. 2, and phonon band structures, colored by their directional mode Grüneisen parameters ($\gamma_{ij,n,\mathbf{k}}$), are shown in Fig. 3. Thermal expansion results from the anharmonicity of both acoustic bands and low-energy optic bands, predominantly those with energies below 200 cm^{-1}. The small mode Grüneisen parameters for perturbations along **b** [Fig. 3(b)] indicate that the large thermal expansion in this direction is driven by elastic anisotropy, as the directional thermal expansion is inversely proportional to the directional Young's modulus [Eq. (2)] and the directional Young's modulus is minimal along **b** [Fig. 2(b)]. Indeed, in the **ab** plane the directional Young's modulus of α-BiB_3O_6 exhibits the bow-tie shape characteristic of flexible framework materials with highly anisotropic thermal expansion, with maxima in Y_{ii} close to minima in $|\alpha_{ii}|$ [Figs. 1(b) and 1(d)] [29,47–49].

The origins of anomalous thermal expansion in α-BiB_3O_6 can be understood further by inspection of the eigenvectors of modes with large mode Grüneisen parameters. The complete set of eigenvectors are available in the Supplemental Material

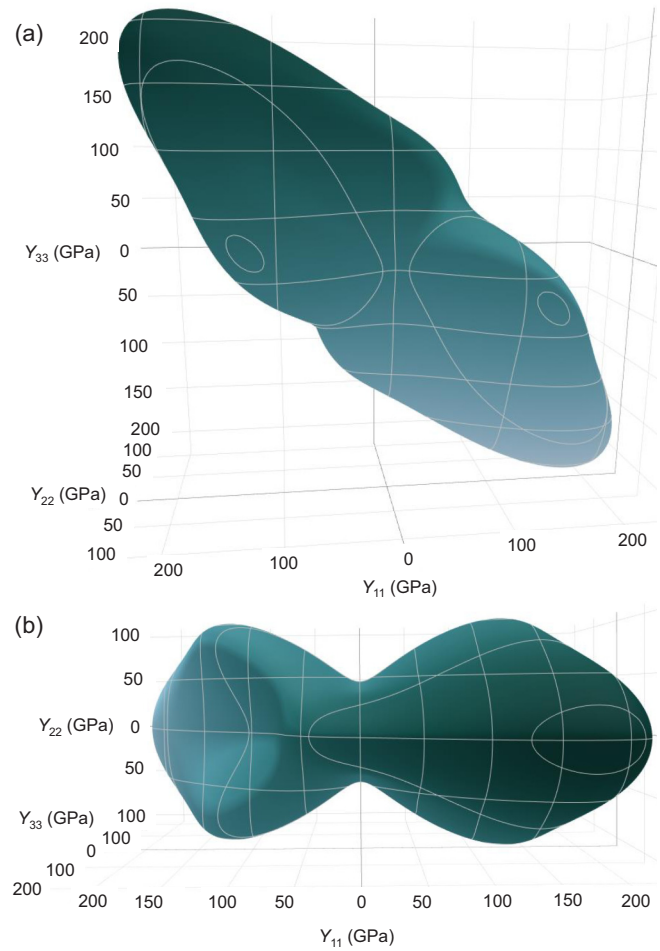

FIG. 2. Calculated directional Young's modulus (Y_{ii}) of α-BiB_3O_6, shown as a blue surface. The views of the **ac** (a) and **ab** (b) planes correspond to Fig. 1. Visualization generated with ELATE [46].

[36], in a format which allows their visualization in animated form [51]. The eigenvectors show that thermal expansion in α-BiB_3O_6 is driven primarily by two types of low-energy phonons: those which involve large displacements of the Bi atoms [Figs. 4(a), 4(c) and 4(d)], and those which primarily involve motions of rigid BO_3 triangles and BO_4 tetrahedra [Figs. 4(b) and 4(e)]. The modes in this latter group are rocking motions of O atoms in the B–O–B bonds [Fig. 4(b)] and the Bi–O–B bonds [Fig. 4(e)]. Such librations of bridging atoms are known to be a common mechanism of NTE in flexible framework materials [9,10].

The low-energy acoustic phonons which drive positive thermal expansion along **b**, and contribute significantly to negative thermal expansion along **a**, involve large displacements of the Bi atoms as well as smaller transverse motions of the borate framework. In some of these modes the Bi atoms oscillate along a linear trajectory [Fig. 4(a)], in others the Bi atoms revolve about their average positions [Figs. 4(c) and 4(d)]. These revolutions follow elliptical orbits due to the anisotropic coordination environment of the Bi atoms [Fig. 1(a)]. Acoustic modes have been found to contribute to NTE in 1D materials [10,52] and in the metal-organic

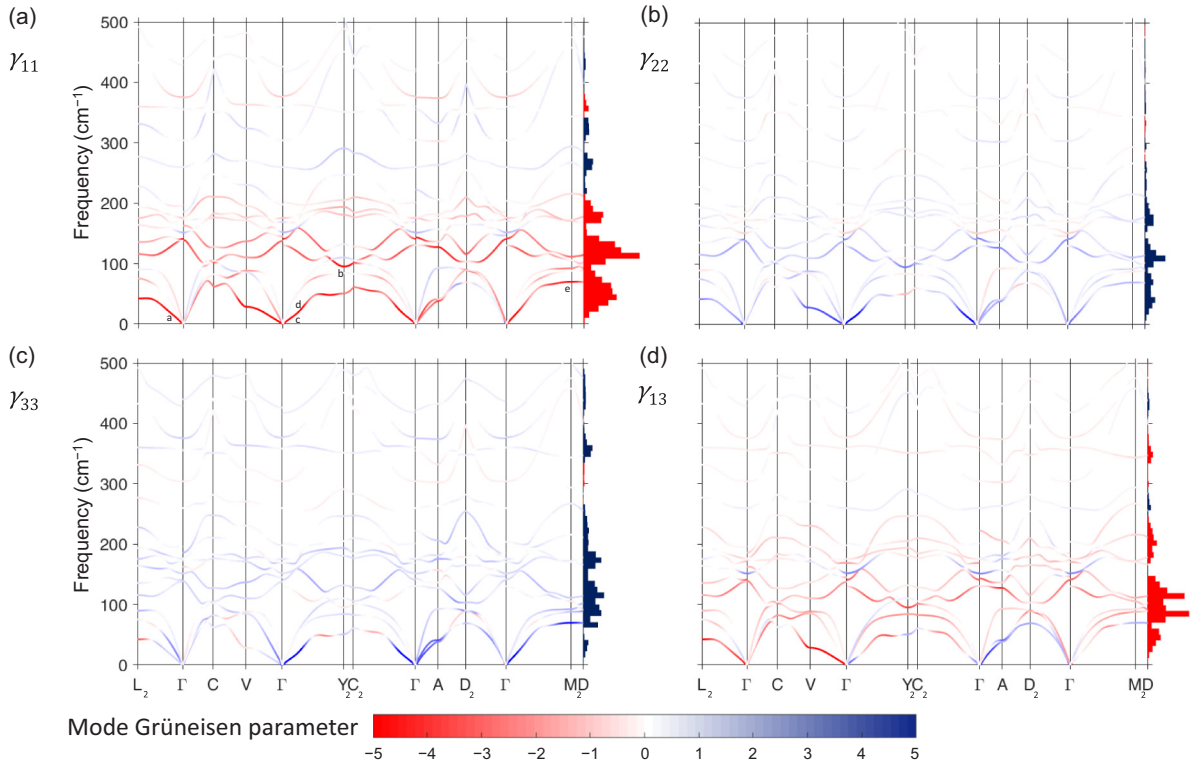

FIG. 3. Phonon band structure of α-BiB_3O_6, with bands colored according to their directional mode Grüneisen parameters ($\gamma_{ij,n,\mathbf{k}}$), calculated using the method of Ref. [29]. Phonons with energies greater than 500 cm^{-1} do not contribute significantly to thermal expansion and are not shown. The density of states (ρ), weighted by the Grüneisen parameters as $\sum_{\mathbf{k}} \rho_{\mathbf{k}}(\omega)\gamma_{ij,\mathbf{k}}(\omega)$, is shown as a histogram at the right of each plot, with positive values colored in blue and negative values in red. Special points in the Brillouin zone were selected following Ref. [50]. The modes marked a–e are visualized in Figs. 4(a)–4(e).

framework MOF-5 [53], although the mechanism in those cases simply involves sinusoidal oscillation of chains or layers, respectively. In α-BiB_3O_6, these transverse displacements are present in the borate layers, and are strongly coupled to the circular motions of the Bi atoms. The elliptical motion of the Bi atom shown in Fig. 4(c) is associated with a larger transverse displacement of the borate layer than the opposing revolution shown in Fig. 4(d). These modes are chiral; the coordinated rotation of the Bi atoms has a distinct handedness and a circular polarization results.

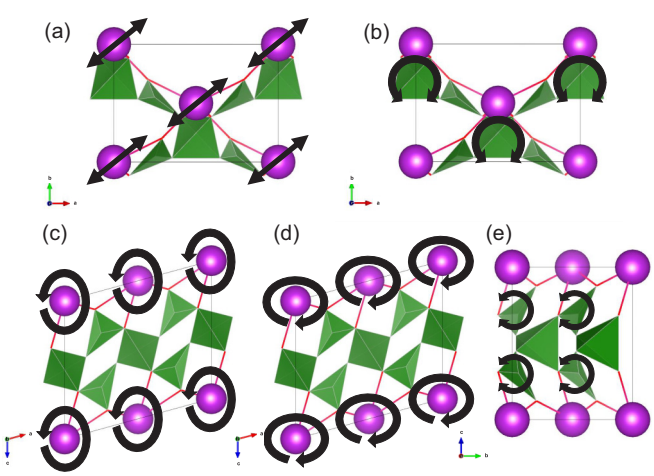

FIG. 4. Cartoon view of the eigenvectors of several phonons in α-BiB_3O_6: linear oscillations of Bi atoms (a); librations of BO_4 tetrahedra (b); elliptical revolutions of Bi atoms about their average positions [(c),(d)]; librations of BO_3 triangles (e) (see Figs. 3 and 5 for mode wave vectors and energies). In order to allow viewing of these modes, animations have been provided in the Supplemental Material [36].

The circular polarization (**S**) of a phonon can be quantified by performing a series of basis transformations to its eigenvectors ($|\epsilon\rangle$) so that each sublattice has a right- or left-handed circular polarization with respect to a given axis [11]. This method has previously been applied to one- and two-dimensional materials [11,12,19]; to examine phonon chirality in α-BiB_3O_6 it was generalized by determining the polarization along each Cartesian axis independently. The new bases are defined, for example for a polarization along **b**, as $|R_{1,22}\rangle \equiv \frac{1}{\sqrt{2}}(i\ 0\ 1\ \cdots\ 0)^{\mathrm{T}}$, $|L_{1,22}\rangle \equiv \frac{1}{\sqrt{2}}(-i\ 0\ 1\ \cdots\ 0)^{\mathrm{T}}$, $|R_{n,22}\rangle \equiv \frac{1}{\sqrt{2}}(0\ \cdots\ i\ 0\ 1)^{\mathrm{T}}$, and $|L_{n,22}\rangle \equiv \frac{1}{\sqrt{2}}(0\ \cdots\ -i\ 0\ 1)^{\mathrm{T}}$, where n is the number of atoms [11,12]. The phonon polarization along **b** (S_{22}) is then the sum of the polarizations of each sublattice:

$$S_{22} = \sum_{\alpha=1}^{n} (|\langle R_{\alpha,22}|\epsilon\rangle|^2 - |\langle L_{\alpha,22}|\epsilon\rangle|^2)\hbar; \tag{3}$$

the circular polarizations S_{11} and S_{33} are obtained by rotation of the basis vectors [11,12].

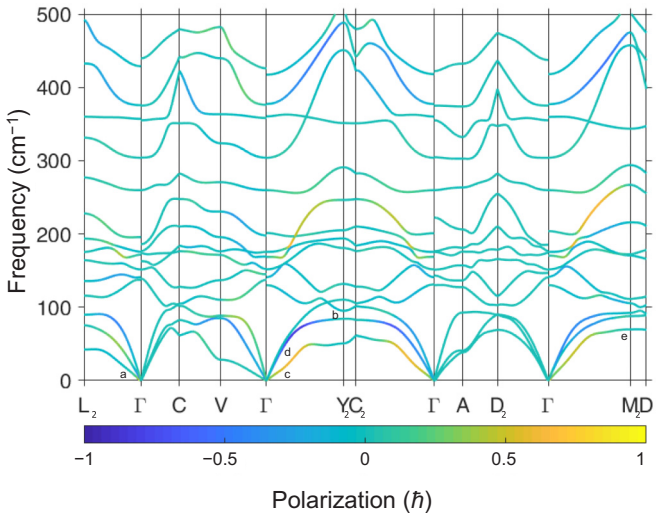

FIG. 5. Phonon band structure of α-BiB_3O_6, with bands colored according to their circular polarizations along **b** (S_{22}). A polarization of $\hbar$ corresponds to a fully right-polarized phonon [11]. Special points in the Brillouin zone were selected following Ref. [50]. The modes marked a–e are visualized in Figs. 4(a)–4(e).

The circular polarizations along **b** of the low-energy phonons are shown in Fig. 5 (the polarizations along the orthogonal axes are shown in the Supplemental Material [36]). A comparison of Figs. 3 and 5 shows that phonon chirality can significantly influence the mode Grüneisen parameters. The transverse acoustic branches can have opposite chirality (e.g., along $\Gamma \rightarrow C_2$), with one branch involving right-handed revolutions of Bi atoms [Fig. 4(c)] and the other having left-handed revolutions [Fig. 4(d)]. The right-handed branch couples strongly to the lattice strains, as evidenced by its large mode Grüneisen parameters, while the left-handed branch does not couple significantly. Note that the two branches do not simply mirror each other; branches with the same energies but reversed chirality exist along paths related by time-reversal symmetry, e.g., $\Gamma \rightarrow C_2'$ [11,50]. Specific signs of the phonon polarization do not lead to specific mode Grüneisen parameters; the chirality is important because the polarized modes correspond to motions which would be symmetry forbidden for phonon eigenvectors in an achiral lattice.

Figures 3 and 5 show that the acoustic modes with circular polarization along **b** are significant contributors to the anomalous thermal expansion of α-BiB_3O_6, as they have large values of γ_{11}, γ_{22}, and γ_{33}. These mode Grüneisen parameters are strongly influenced by dispersive interactions, as their signs and magnitudes vary widely between calculations including a dispersion correction (Fig. 3) and those performed without it (see the Supplemental Material [36]). This discrepancy suggests that the qualitative level of accuracy in the calculated CTE could be due to underestimation of the Grüneisen parameters of the chiral modes.

The relationship between phonon chirality and thermal expansion in α-BiB_3O_6 can be understood by examination of the chiral acoustic modes. If the structure of α-BiB_3O_6 were achiral, adjacent Bi atoms would be required to revolve in opposite directions in order to maintain zero circular polarization [11,12]. Therefore, modes which involve such elliptical motions are limited to the edges of the Brillouin zone in achiral crystals. As Fig. 3 shows, the modes that contribute most strongly to thermal expansion lie away from the edges of the Brillouin zone. Therefore, revolutions of Bi atoms with small wave vectors couple strongly to the lattice strains, and if such phonons were disallowed by symmetry, the thermal expansion of α-BiB_3O_6 would be less extreme. Chirality therefore acts like a degree of freedom, or as a kind of flexibility: it allows a specific type of low-energy phonon in α-BiB_3O_6, analogously to how corner-linked topologies of coordination polyhedra can allow low-energy rigid unit modes (RUMs) to exist [10]. Since the chiral phonons can have negative mode Grüneisen parameters, it is possible for them to act as soft modes and cause pressure-induced phase transitions [10,54].

The chiral nature of α-BiB_3O_6 is quite unusual among inorganic framework materials, and here the connection between that unusual structural feature and the phonons which cause anomalous thermal expansion has been revealed. It is interesting to note that, despite the general rarity of chiral inorganic crystals, several very prominent NTE materials crystallize in chiral space groups: α-ZrW_2O_8, which was the first material discovered to have isotropic NTE over a broad temperature range, crystallizes in $P2_13$ [55], and β-eucryptite, which is widely used in zero-thermal-expansion glass ceramics, adopts $P6_422$ [56]. The structure of β-eucryptite is identical to that of β-quartz, which also displays NTE [57].

The chiral modes found in α-BiB_3O_6 are distinct from the RUMs which have been used successfully to understand NTE in some materials [10]. However, the RUM model has been found to not apply to many NTE materials, either because of overconstraint of coordination polyhedra [58], or because the polyhedra simply are not rigid [59,60]. In materials where the RUM model fails, the origins of NTE often remain incompletely understood, and it is possible that, for chiral systems, calculations of mode circular polarizations could bring additional clarity.

In α-ZrW_2O_8, NTE is caused by a wide range of low-energy modes involving motions of rigid WO_4 tetrahedra and Zr–O bonds [59,61]. These modes can be described as fluctuations towards denser structures where nonbridging O atoms on WO_4 tetrahedra form W–O–W chains [60,62]. The rigidity constraints could allow chiral motions of the Zr atoms and of the nonbridging O atoms on the WO_4 tetrahedra. For example, a revolution of a terminal O atom would bring it closer in turn to each of the three equivalent positions where it could form a W–O–W link [60]. As the terminal O atoms are permitted by network topology and crystallographic symmetry to undergo chiral revolutions, it would not be surprising to find such modes with the methods used here.

In conclusion, two types of phonons were found to contribute significantly to thermal expansion in α-BiB_3O_6: motions of the rigid borate units, and modes involving oscillations and revolutions of the bismuth atoms. These revolutions correspond to chiral acoustic phonons; along certain directions in reciprocal space the two transverse acoustic branches have opposite circular polarizations, with only one coupling strongly to the lattice strains. Were the lattice achiral, such modes would be disallowed by symmetry except at the edges

of the Brillouin zone, where they have small mode Grüneisen parameters. Phonon chirality has therefore been related to the macroscopic behavior of a three-dimensional material, demonstrating that structural chirality permits specific types of modes in a manner analogous to structural flexibility. The resulting chrial phonons have low energies and large mode Grüneisen parameters; they thereby drive thermal expansion and potentially could act as soft modes and cause phase transitions. This result reveals a connection between the absence of a particular type of crystallographic symmetry and an emergent physical property, and can be applied to the study of structure–property relationships in other chiral crystals.

The author acknowledges the support of the National Sciences and Engineering Council of Canada. Computational resources were provided by the University of Oxford, Department of Chemistry, and the UK's HEC Materials Chemistry Consortium, which is funded by EPSRC (EP/L000202). This work used the ARCHER UK National Supercomputing Service.

[1] H. Hellwig, J. Liebertz, and L. Bohatý, Exceptional large nonlinear optical coefficients in the monoclinic bismuth borate BiB_3O_6 (BIBO), Solid State Commun. **109**, 249 (1998).

[2] O. Pinel, P. Jian, R. M. de Araújo, J. Feng, B. Chalopin, C. Fabre, and N. Treps, Generation and Characterization of Multimode Quantum Frequency Combs, Phys. Rev. Lett. **108**, 083601 (2012).

[3] L.-K. Chen, Z.-D. Li, X.-C. Yao, M. Huang, W. Li, H. Lu, X. Yuan, Y.-B. Zhang, X. Jiang, C.-Z. Peng *et al.*, Observation of ten-photon entanglement using thin BiB_3O_6 crystals, Optica **4**, 77 (2017).

[4] X.-L. Wang, L.-K. Chen, W. Li, H.-L. Huang, C. Liu, C. Chen, Y.-H. Luo, Z.-E. Su, D. Wu, Z.-D. Li *et al.*, Experimental Ten-Photon Entanglement, Phys. Rev. Lett. **117**, 210502 (2016).

[5] B. Teng, Z. Wang, H. Jiang, X. Cheng, H. Liu, X. Hu, S. Dong, J. Wang, and Z. Shao, Anisotropic thermal expansion of BiB_3O_6, J. Appl. Phys. **91**, 3618 (2002).

[6] W.-D. Stein, A. Cousson, P. Becker, L. Bohatý, and M. Braden, Temperature-dependent X-ray and neutron diffraction study of BiB_3O_6, Z. Kristallogr. **222**, 680 (2007).

[7] L. Kang, X. Jiang, S. Luo, P. Gong, W. Li, X. Wu, Y. Li, X. Li, C. Chen, and Z. Lin, Negative linear compressibility in a crystal of α-BiB_3O_6, Sci. Rep. **5**, 13432 (2015).

[8] A. B. Cairns and A. L. Goodwin, Negative linear compressibility, Phys. Chem. Chem. Phys. **17**, 20449 (2015).

[9] C. P. Romao, K. J. Miller, C. A. Whitman, M. A. White, and B. A. Marinkovic, Negative thermal expansion (thermomiotic) materials, in *Comprehensive Inorganic Chemistry II* (Elsevier, New York, 2013), pp. 127–151.

[10] M. T. Dove and H. Fang, Negative thermal expansion and associated anomalous physical properties: Review of the lattice dynamics theoretical foundation, Rep. Prog. Phys. **79**, 066503 (2016).

[11] L. Zhang and Q. Niu, Chiral Phonons at High-Symmetry Points in Monolayer Hexagonal Lattices, Phys. Rev. Lett. **115**, 115502 (2015).

[12] M. Gao, W. Zhang, and L. Zhang, Nondegenerate chiral phonons in graphene/hexagonal boron nitride heterostructure from first-principles calculations, Nano Lett. **18**, 4424 (2018).

[13] H. Zhu, J. Yi, M.-Y. Li, J. Xiao, L. Zhang, C.-W. Yang, R. A. Kaindl, L.-J. Li, Y. Wang, and X. Zhang, Observation of chiral phonons, Science **359**, 579 (2018).

[14] C. Strohm, G. L. J. A. Rikken, and P. Wyder, Phenomenological Evidence for the Phonon Hall Effect, Phys. Rev. Lett. **95**, 155901 (2005).

[15] L. Zhang and Q. Niu, Angular Momentum of Phonons and the Einstein–de Haas Effect, Phys. Rev. Lett. **112**, 085503 (2014).

[16] D. M. Juraschek and N. A. Spaldin, Orbital magnetic moments of phonons, Phys. Rev. Mater. **3**, 064405 (2019).

[17] T. Nomura, X.-X. Zhang, S. Zherlitsyn, J. Wosnitza, Y. Tokura, N. Nagaosa, and S. Seki, Phonon Magnetochiral Effect, Phys. Rev. Lett. **122**, 145901 (2019).

[18] M. Hamada, E. Minamitani, M. Hirayama, and S. Murakami, Phonon Angular Momentum Induced by the Temperature Gradient, Phys. Rev. Lett. **121**, 175301 (2018).

[19] T. Pandey, C. A. Polanco, V. R. Cooper, D. S. Parker, and L. Lindsay, Symmetry-driven phonon chirality and transport in one-dimensional and bulk Ba_3N-derived materials, Phys. Rev. B **98**, 241405(R) (2018).

[20] C. A. Kennedy and M. A. White, Unusual thermal conductivity of the negative thermal expansion material, ZrW_2O_8, Solid State Commun. **134**, 271 (2005).

[21] L. Wang, C. Wang, H. Luo, and Y. Sun, Correlation between uniaxial negative thermal expansion and negative linear compressibility in $Ag_3[Co(CN)_6]$, J. Phys. Chem. C **121**, 333 (2016).

[22] A. L. Goodwin, M. Calleja, M. J. Conterio, M. T. Dove, J. S. O. Evans, D. A. Keen, L. Peters, and M. G. Tucker, Colossal positive and negative thermal expansion in the framework material $Ag_3[Co(CN)_6]$, Science **319**, 794 (2008).

[23] M. K. Gupta, B. Singh, R. Mittal, M. Zbiri, A. B. Cairns, A. L. Goodwin, H. Schober, and S. L. Chaplot, Anomalous thermal expansion, negative linear compressibility, and high-pressure phase transition in $ZnAu_2(CN)_4$: Neutron inelastic scattering and lattice dynamics studies, Phys. Rev. B **96**, 214303 (2017).

[24] M. S. Senn, A. Bombardi, C. A. Murray, C. Vecchini, A. Scherillo, X. Luo, and S. W. Cheong, Negative Thermal Expansion in Hybrid Improper Ferroelectric Ruddlesden-Popper Perovskites by Symmetry Trapping, Phys. Rev. Lett. **114**, 035701 (2015).

[25] E. T. Ritz and N. A. Benedek, Interplay Between Phonons and Anisotropic Elasticity Drives Negative Thermal Expansion in $PbTio_3$, Phys. Rev. Lett. **121**, 255901 (2018).

[26] C. P. Romao, F. A. Perras, U. Werner-Zwanziger, J. A. Lussier, K. J. Miller, C. M. Calahoo, J. W. Zwanziger, M. Bieringer, B. A. Marinkovic, D. L. Bryce, and M. A. White, Zero thermal expansion in $ZrMgMo_3O_{12}$: NMR crystallography reveals origins of thermoelastic properties, Chem. Mater. **27**, 2633 (2015).

[27] S. Bhattacharya and B. K. Saha, Uniaxial negative thermal expansion in an organic complex caused by sliding of layers, Cryst. Growth Des. **12**, 4716 (2012).

[28] B. K. Saha, Thermal expansion in organic crystals, J. Indian Inst. Sci. **97**, 177 (2017).

[29] C. P. Romao, Anisotropic thermal expansion in flexible materials, Phys. Rev. B **96**, 134113 (2017).

[30] X. Gonze and C. Lee, Dynamical matrices, Born effective charges, dielectric permittivity tensors, and interatomic force constants from density-functional perturbation theory, Phys. Rev. B **55**, 10355 (1997).

[31] B. Van Troeye, M. Torrent, and X. Gonze, Interatomic force constants including the DFT-D dispersion contribution, Phys. Rev. B **93**, 144304 (2016).

[32] X. Gonze, F. Jollet, F. A. Araujo, D. Adams, B. Amadon, T. Applencourt, C. Audouze, J.-M. Beuken, J. Bieder, A. Bokhanchuk *et al.*, Recent developments in the ABINIT software package, Comput. Phys. Commun. **205**, 106 (2016).

[33] F. Bottin, S. Leroux, A. Knyazev, and G. Zérah, Large-scale ab initio calculations based on three levels of parallelization, Comput. Mater. Sci. **42**, 329 (2008).

[34] T. Björkman, CIF2cell: Generating geometries for electronic structure programs, Comput. Phys. Commun. **182**, 1183 (2011).

[35] M. Torrent, F. Jollet, F. Bottin, G. Zérah, and X. Gonze, Implementation of the projector augmented-wave method in the ABINIT code: Application to the study of iron under pressure, Comput. Mater. Sci. **42**, 337 (2008).

[36] See Supplemental Material at http://link.aps.org/supplemental/10.1103/PhysRevB.100.060302 for example DFT input files, further description of computational methods, thermal expansion tensors, elastic tensors, mode Grüneisen parameters calculated without dispersion correction, phonon circular polarizations, animations of several important phonon modes, and phonon eigenvectors in JSON format.

[37] W. Kohn and L. J. Sham, Self-consistent equations including exchange and correlation effects, Phys. Rev. **140**, A1133 (1965).

[38] L. He, F. Liu, G. Hautier, M. J. T. Oliveira, M. A. L. Marques, F. D. Vila, J. J. Rehr, G.-M. Rignanese, and A. Zhou, Accuracy of generalized gradient approximation functionals for density-functional perturbation theory calculations, Phys. Rev. B **89**, 064305 (2014).

[39] S. Grimme, J. Antony, S. Ehrlich, and H. Krieg, A consistent and accurate *ab initio* parametrization of density functional dispersion correction (DFT-D) for the 94 elements H-Pu, J. Chem. Phys. **132**, 154104 (2010).

[40] A. D. Becke and E. R. Johnson, A simple effective potential for exchange, J. Chem. Phys. **124**, 221101 (2006).

[41] J. P. Perdew, K. Burke, and M. Ernzerhof, Generalized Gradient Approximation Made Simple, Phys. Rev. Lett. **77**, 3865 (1996).

[42] D. R. Hamann, Optimized norm-conserving Vanderbilt pseudopotentials, Phys. Rev. B **88**, 085117 (2013).

[43] H. J. Monkhorst and J. D. Pack, Special points for Brillouin-zone integrations, Phys. Rev. B **13**, 5188 (1976).

[44] psps tables|ABINIT, https://www.abinit.org/psp-tables, accessed: 2017-01-20.

[45] SG15 ONCV potentials, http://www.quantum-simulation.org/potentials/sg15_oncv/, accessed: 2017-01-20.

[46] R. Gaillac, P. Pullumbi, and F.-X. Coudert, ELATE: An open-source online application for analysis and visualization of elastic tensors, J. Phys.: Condens. Matter **28**, 275201 (2016).

[47] A. U. Ortiz, A. Boutin, A. H. Fuchs, and F.-X. Coudert, Anisotropic Elastic Properties of Flexible Metal-Organic Frameworks: How Soft are Soft Porous Crystals?, Phys. Rev. Lett. **109**, 195502 (2012).

[48] A. U. Ortiz, A. Boutin, A. H. Fuchs, and F.-X. Coudert, Metal–organic frameworks with wine-rack motif: What determines their flexibility and elastic properties?, J. Chem. Phys. **138**, 174703 (2013).

[49] K. Dolabdjian, A. Kobald, C. P. Romao, and H.-J. Meyer, Synthesis and thermoelastic properties of $(ZrCN_2)_2$ and $(HfCN_2)_2$, Dalton Trans. **47**, 10249 (2018).

[50] Y. Hinuma, G. Pizzi, Y. Kumagai, F. Oba, and I. Tanaka, Band structure diagram paths based on crystallography, Comput. Mater. Sci. **128**, 140 (2017).

[51] Phonon visualization website, http://henriquemiranda.github.io/phonon-visualization-website.html, accessed: 2018-11-16.

[52] H. Fang, M. T. Dove, and A. E. Phillips, Common origin of negative thermal expansion and other exotic properties in ceramic and hybrid materials, Phys. Rev. B **89**, 214103 (2014).

[53] L. H. N. Rimmer, M. T. Dove, A. L. Goodwin, and D. C. Palmer, Acoustic phonons and negative thermal expansion in MOF-5, Phys. Chem. Chem. Phys. **16**, 21144 (2014).

[54] R. E. Dinnebier, B. Hinrichsen, A. Lennie, and M. Jansen, High-pressure crystal structure of the non-linear optical compound BiB_3O_6 from two-dimensional powder diffraction data, Acta Crystallogr., Sect. B: Struct. Sci., Cryst. Eng. Mater. **65**, 1 (2009).

[55] T. A. Mary, J. S. O. Evans, T. Vogt, and A. W. Sleight, Negative thermal expansion from 0.3 to 1050 Kelvin in ZrW_2O_8, Science **272**, 90 (1996).

[56] A. I. Lichtenstein, R. O. Jones, H. Xu, and P. J. Heaney, Anisotropic thermal expansion in the silicate β-eucryptite: A neutron diffraction and density functional study, Phys. Rev. B **58**, 6219 (1998).

[57] P. R. L. Welche, V. Heine, and M. T. Dove, Negative thermal expansion in beta-quartz, Phys. Chem. Minerals **26**, 63 (1998).

[58] L. H. N. Rimmer and M. T. Dove, Simulation study of negative thermal expansion in yttrium tungstate $Y_2W_3O_{12}$, J. Phys.: Condens. Matter **27**, 185401 (2015).

[59] L. H. N. Rimmer, M. T. Dove, and K. Refson, The negative thermal expansion mechanism of zirconium tungstate, ZrW_2O_8, arXiv:1510.00361.

[60] M. Baise, P. M. Maffettone, F. Trousselet, N. P. Funnell, F.-X. Coudert, and A. L. Goodwin, Negative Hydration Expansion in ZrW_2O_8: Microscopic Mechanism, Spaghetti Dynamics, and Negative Thermal Expansion, Phys. Rev. Lett. **120**, 265501 (2018).

[61] M. K. Gupta, R. Mittal, and S. L. Chaplot, Negative thermal expansion in cubic ZrW_2O_8: Role of phonons in the entire Brillouin zone from *ab initio* calculations, Phys. Rev. B **88**, 014303 (2013).

[62] J. S. O. Evans, Z. Hu, J. D. Jorgensen, D. N. Argyriou, S. Short, and A. W. Sleight, Compressibility, phase transitions, and oxygen migration in zirconium tungstate, ZrW_2O_8, Science **275**, 61 (1997).